Eur. Phys. J. Special Topics **166**, 7–10 (2009)

DOI: 10.1140/epjst/e2009-00869-y

THE EUROPEAN PHYSICAL JOURNAL SPECIAL TOPICS

Regular Article

Vibrations of sessile drops

X. Noblin[1,a], A. Buguin[2], and F. Brochard-Wyart[2]

[1] Laboratoire de Physique de la Matière Condensée, UMR 6622, CNRS – Université de Nice Sophia-Antipolis, Parc Valrose 06108 Nice Cedex 2, France
[2] Institut Curie, UMR 168, CNRS – Université Pierre et Marie Curie, 26 rue d'Ulm, 75248 Paris, France

Abstract. This study focuses on the effects of vertical vibrations on sessile drops deposited on hydrophobic substrates. At low amplitudes the contact line remains pinned because of contact angle hysteresis and only drop surface modes are observed. Above a first threshold the contact line starts to move and exhibits a stick-slip behavior that presents some analogies with the solid friction on a mechanical oscillator. At larger amplitudes, non-axisymmetric contour modes show up (modes m = 2, 3...). They can be interpreted as a coupling between surface modes and contact line motion. These subharmonic modes are well described within the framework of parametric oscillators. We also discuss here why vibrations can help to measure equilibrium contact angle.

1 Introduction

The study of oscillations present at the surface of free liquid drops is a classical problem [1,2]. But, more recently, articles concerning vibrations of supported drops have focused attention due to their potential applications for crystal growth [3], atomization [4] and droplets manipulations [5,6] (see [7] and references therein). In [5,6] substrates are submitted to horizontal vibrations, which can lead to drop motion when the excitation is non sinusoidal. Here we focused on vertical vibrations and the response of a sessile drop lying on a solid substrate with a moderate contact angle hysteresis (defined as the difference between the *cosine* of receding and advancing contact angles: $H = \cos(\theta_r) - \cos(\theta_a)$). Drop size ranges from mm to cm radii, the bigger drops are then flattened by gravity. For increasing amplitude of vibration, and depending on the frequency, we observed three successive types of modes. We describe axisymmetric modes with fixed (section 2) then moving contact line (section 3). In section 4, we discuss the application to contact angle measurements and in section 5 the non axisymmetric (contour) modes.

2 Axisymmetric modes: Fixed contact line

Substrates made of polystyrene ($\theta_a = 92°$, $\theta_r = 78°$) or Teflon ($\theta_a = 125°$, $\theta_r = 115°$) were placed in a closed vessel to reduce evaporation and contamination effects. They were attached to the moving part of a loudspeaker (driven by a function generator and a power amplifier) giving a periodic acceleration (frequency f_E between $5-100$ Hz): $a = -(2\pi f_E)^2 u_0 \cos(2\pi f_E t)$, where u_0 corresponds to the amplitude of motion (Fig. 1(b)).

At low amplitude of vibrations, drops (ultra pure water) exhibited forced oscillations at the same frequency as excitation. We measured response spectra, looking at the surface slope

[a] e-mail: xavier.noblin@unice.fr

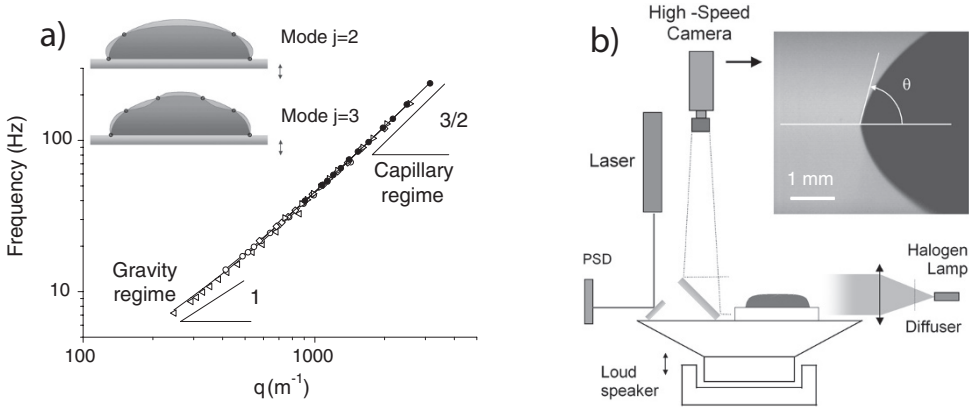

Fig. 1. (a) Resonant frequencies for fixed contact line modes. (◁) j = 2, (○) j = 3, (◇) j = 4, (▷) j = 5 and (●) j = 6. The straight line represents our wave model. (b) Moving contact line mode experimental setup.

oscillations using the refraction of a laser beam, by Fourier transform of a white noise excitation, normalized by the acceleration. This gave us successive narrow peaks corresponding to resonant frequencies (mode j = 2, 3 . . .) [7]. j is half the number of nodes along the drop profile (Fig. 1(a)).

These modes can be seen as stationary surface waves, their exact calculations have been made in the capillary regime [8]. In our case, drop can be flattened by gravity, to simplify the problem and to have a simple prediction for the eigen frequencies values, we assume that the mode wavelengths are: $\lambda_j = \frac{2\pi}{q_j} = \frac{2p}{(j-1/2)}$, p is the meridian drop profile length. We calculate p as a function of the drop volume using numerical integration of the drop profile. From the 1D dispersion relation of capillary-gravity waves on a liquid bath of depth h (here the mean height is: $h_m = \frac{V}{\pi R^2}$), we found [2]: $\omega_j^2 = (gq_j + \frac{\gamma}{\rho} q_j^3) \tanh(q_j \frac{V}{\pi R^2})$.

We have traced $\omega(q)$ (Fig. 1). Our prediction with the model is satisfactory, except for the first mode ($j = 2$), where the discrepancy reaches 8% for the drop sizes studied.

3 Axisymmetric modes: Moving contact line

At higher excitation amplitudes, the contact angle variations can exceed the contact angle hysteresis, putting the contact line into motion. These modes were imaged (side view) with a high speed camera (1000 image/s). The axis of view is slightly tilted (3° above horizontal): we see the drop profile and its reflection on the substrate (see Fig. 1(b)). By image analysis, we calculated the contact angle value and the contact line position. We used a sinusoidal signal to obtain spectra for the radius and contact angle oscillation amplitude as function of frequency.

We could check that the contact line starts to move when the contact angle variation ($\Delta\theta$) becomes larger than $\theta_a - \theta_r$: the vibrations overcome hysteresis. At low acceleration amplitude, the contact line moves only for frequencies close to the pinned modes resonance. In large frequency domains, the contact line remains pinned by the substrate. The motion is complex and presents a stick-slip behavior: the contact line is pinned during a part of the time (stick), then it advances (slip), stops for a while (stick), goes back (slip) and so on. This behavior can be explain by the force of hysteresis, which acts as a "solid friction" on the moving line.

The drop behaves like an oscillator with solid friction, ruled by the equation: $\ddot{x} + \omega_0^2 x + \mu\, sgn(\dot{x}) = A\cos(\omega t)$ (see [7] for details, $x = R - R_{eq}$). Where μ is the solid friction coefficient (proportional to H), $sgn(u)$ is the function (± 1) sign of u. ω_0 is the natural frequency of the oscillator. Such system has been studied for instance in [9]. Authors found different possible motions depending on the ratio A/μ and ω/ω_0, they observed stick-slip motion (with 2 stops per period or more) and also pure slipping oscillatory motion with no stop. We could observe experimentally several features coherent with this forced solid friction oscillator model [7].

This phenomena can be used to suppress the effect of hysteresis using vibrations. It can be selective on the drop size by tuning the frequency. An application is the possibility of displacing drops on a substrate more easily using another force field (electrical for instance). In our case gravity plays this role, when there is a very small tilt of the substrate, drops are displaced quickly, (all the substrates were slightly curved for that reason). From $R(t) - \theta(t)$ curves we can easily measure the velocity curve $v(\theta)$ and probe contact line dynamics, extending classical studies to the inertial regime.

4 Why vibrations can help measuring the equilibrium contact angle?

We discuss here a method to measure equilibrium contact angle θ_E. In [11], vibrations are used empirically with that goal on rough substrates. We propose to make clear why this is possible and how. When one deposits a drop on a horizontal flat solid substrate, the contact angle measured can have any value θ_i belonging to $[\theta_r, \theta_a]$, depending on the way it has been deposited. When such a drop is at rest, with an angle θ it is in mechanical equilibrium, but not necessarily in thermodynamical equilibrium (the system is in a local energy minima, but not in the global one given by $\theta = \theta_E$). Due to volume conservation, there is a non ambiguous relation $R(\theta)$. We can calculate exactly this relation in the two limits: 1) $R \ll \kappa^{-1}$, the drop is a portion a sphere, hence: $R = (3V/(\pi(1-\cos\theta)^2(2+\cos\theta))^{1/3}$. 2) $R \gg \kappa^{-1}$, the drop is a flat puddle (penny shape), hence: $R = \sqrt{V/(2\pi\kappa^{-1}\sin(\theta/2))}$. This means that there is only one value for the radius that corresponds to θ_E: R_E. In the general case, numerical integration for the drop profile is necessary.

The method consists in inducing vibration near a resonance, to put the contact line into a large axisymmetric motion, then to reduce slowly the amplitude until the radius stops to oscillate. The resulting stick slip motion will lead in the plane (R, θ) to a cycle as sketched in Fig. 2(b)), with R constant when $\theta \in [\theta_r, \theta_a]$. The first cycle is represented, then the forcing amplitude is reduced at each period, describing successive cycles with decreasing amplitude in radius. When the drop stops to move, the corresponding point on the diagram is on the $R(\theta)$ curve somewhere inside the last cycle, which can be very small in radius amplitude and lead to an angle very close to θ_E. As mentioned earlier, this is because the drop tends to its thermodynamical equilibrium, which correspond to a global energy minimum, at $\theta = \theta_E$ with the help of vibrations that allow the exploration of the potential energy landscape. Only a few periods are necessary on a smooth substrate.

If large vibrations are stopped too quickly, the θ_E value can be missed. In addition the hysteresis has to be moderate or the contact angle sufficiently high so that the drop can actually be put in motion, if not, the drop will break up into droplets. The choice of the frequency is important to avoid modes that could perturb the drop stop or induce unwanted non-axisymmetric modes as described in the following.

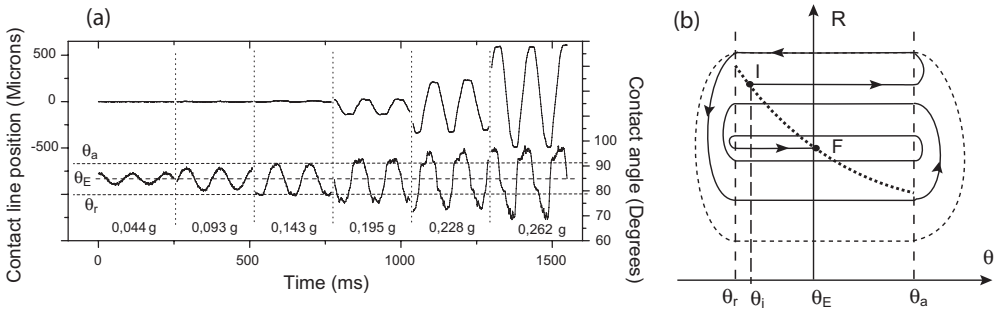

Fig. 2. (a) Contact line position (top) and contact angle (bottom) as a function of time for different accelerations. (b) Cycles during decreasing amplitude from θ_i (I) to θ_E (F) in the (R, θ) plane.

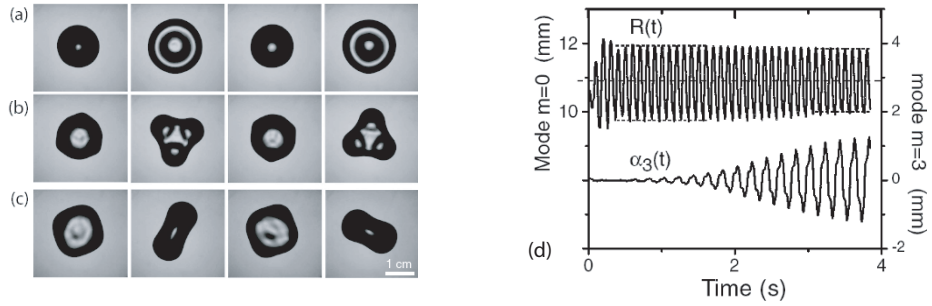

Fig. 3. (a) Mode m = 0, below the threshold, $f_E = 9\,\text{Hz}$. (b) m = 3, $f_E = 9\,\text{Hz}$. (c) m = 2, $f_E = 6\,\text{Hz}$. Frame rate $= 2/f_E$. (d) m = 0 (top) and m = 3 (bottom) amplitudes vs. time, R = 11 mm, $f_E = 10\,\text{Hz}$.

5 Contour modes

We have used the same apparatus as described in section 3 but the high speed camera was used to image the drops from above to measure their contour $R(\theta, t)$ by image analysis. We took the Fourier transform of this function to determine the amplitude of each mode m for each image. For particular frequencies and sufficiently high amplitudes (above the contact line motion threshold) we observed star shaped mode (m = 2, 3, 4 ...). These modes are subharmonic, they are due to an exchange between potential energy stored in the elastic deformation of the contact line and kinetic energy of the moving fluid. This lead to triplons: propagation of wave along the contact line. The vibrations of a drop allow to observe these modes since hysteresis effects are reduced and to excite them parametrically, leading to discrete modes, corresponding to: $U_m(\theta, t) = u_m(t)\cos(m\theta)$. The frequencies are given by [12]: $\omega_m^2 = C\frac{\gamma}{\rho}m(m^2-1)/R^3$, with C a function of θ_E. We see that if R varies with time, we have a parametric oscillator. This happen at sufficiently high oscillation amplitude, assuming $R(t) = R_e + \Delta R\cos(\omega_E t)$, we found in first approximation for a mode $u_m(t)$: $\ddot{u}_m + \omega_m^2(1 + h\cos(\omega_E t))u_m = 0$, with $h = 3\Delta R/R$.

The main oscillation frequency is half the excitation frequency, the instability grows exponentially and the characteristic time associated diverges close to the threshold. Note that the control parameter is $h = 3\Delta R/R$ which makes the coupling with contact line modes complex and highly dependant on frequency, all the modes cannot be observed for a given drop size.

6 Conclusion

Vertical drop vibrations lead to different modes involving surfaces waves, contact line dynamics and parametric instabilities. It can lead to true determination of equilibrium contact angles, complex drop manipulations and allows promising studies on inertial dynamics.

References

1. H. Lamb, *Hydrodynamics* (Cambridge University Press, 1932)
2. L. Landau, M. Lifshitz, *Fluid Mechanics* (1967)
3. C. Bisch, A. Lasek, H. Rodot, J. Méc. Théor. Appl. **1**, 165 (1982)
4. A.J. James, B. Vukasinovic, M.K. Smith, et al., J. Fluid Mech. **476**, 1 (2003)
5. S. Daniel, M.K. Chaudhury, P.G. de Gennes, Langmuir **21**, 4240 (2005)
6. F. Celestini, R. Kofman, Phys. Rev. E **73**, 041602 (2006)
7. X. Noblin, A. Buguin, F. Brochard-Wyart, Eur. Phys. J. E **14**, 395 (2004)
8. M. Strani, F. Sabetta, J. Fluid Mech. **141**, 233 (1984)
9. H.-K. Hong, C.-S. Liu, J. Sound Vibr. **229**, 1171 (2000)
10. C. Andrieu, C. Sykes, F. Brochard, Langmuir **10**, 2077 (1994)
11. T.S. Meiron, A. Marmur, I.S. Saguy, J. Coll. Int. Sci. **274**, 637 (2004)
12. X. Noblin, A. Buguin, F. Brochard-Wyart, Phys. Rev. Lett. **94**, 166102 (2005)